

Natural or Induced: Identifying Natural and Induced Swarms from Pre-production and Co-production Microseismic Catalogs at the Coso Geothermal Field

Martin Schoenball^{1,2}, J. Ole Kaven², Jonathan M.G. Glen² and Nicholas C. Davatzes¹

¹ Earth and Environmental Science, Temple University, Philadelphia, PA

² GMEG Science Center, U.S. Geological Survey, Menlo Park, CA

mschoenball@usgs.gov

Keywords: Coso Geothermal Field, Induced Seismicity, Earthquake Swarms

ABSTRACT

Increased levels of seismicity coinciding with injection of reservoir fluids have prompted interest in methods to distinguish induced from natural seismicity. Discrimination between induced and natural seismicity is especially difficult in areas that have high levels of natural seismicity, such as the geothermal fields at the Salton Sea and Coso, both in California. Both areas show swarm-like sequences that could be related to natural, deep fluid migration as part of the natural hydrothermal system. Therefore, swarms often have spatio-temporal patterns that resemble fluid-induced seismicity, and might possibly share other characteristics.

The Coso Geothermal Field and its surroundings is one of the most seismically active areas in California with a large proportion of its activity occurring as seismic swarms. Here we analyze clustered seismicity in and surrounding the currently produced reservoir comparatively for pre-production and co-production periods. We perform a cluster analysis, based on the inter-event distance in a space-time-energy domain to identify notable earthquake sequences. For each event j , the closest previous event i is identified and their relationship categorized. If this nearest neighbor's distance is below a threshold based on the local minimum of the bimodal distribution of nearest neighbor distances, then the event j is included in the cluster as a child to this parent event i . If it is above the threshold, event j begins a new cluster. This process identifies subsets of events whose nearest neighbor distances and relative timing qualify as a cluster as well as a characterizing the parent-child relationships among events in the cluster.

We apply this method to three different catalogs: (1) a two-year microseismic survey of the Coso geothermal area that was acquired before exploration drilling in the area began; (2) the HYS_catalog_2013 that contains 52,000 double-difference relocated events and covers the years 1981 to 2013; and (3) a catalog of 57,000 events with absolute locations from the local network recorded between 2002 and 2007. Using this method we identify 10 clusters of more than 20 events each in the pre-production survey and more than 200 distinct seismicity clusters that each contain at least 20 and up to more than 1000 earthquakes in the more extensive catalogs.

The cluster identification method used yields a hierarchy of links between multiple generations of parent and offspring events. We analyze different topological parameters of this hierarchy to better characterize and thus differentiate natural swarms from induced clustered seismicity and also to identify aftershock sequences of notable mainshocks. We find that the branching characteristic given by the average number of child events per parent event is significantly different for clusters below than for clusters around the produced field.

1. INTRODUCTION

Mitigating and controlling induced seismicity is a key challenge in future large-scale application of geothermal energy [IEA, 2011]. Several geothermal projects have experienced unexpected levels of induced seismicity during drilling, stimulation or subsequent circulation [Majer *et al.*, 2007; Zang *et al.*, 2014], leading to abandonment of projects or requiring reduced production. Similarly, a growing number of confirmed cases of seismicity induced through waste water disposal [Ellsworth, 2013] have created a strong demand to recognize induced seismicity during active injection or production and to find methods to distinguish it from natural seismicity. Early identification will more clearly define the activities and mechanisms that initiate and control the characteristics of resulting events. Such recognition would serve the dual purpose of developing better tools for mitigating damaging earthquakes as well as for providing a firmer basis to understand the role of earthquakes in reservoir and crustal permeability. Controversy arises where seismically very active systems are subjected to strong man-made perturbation, e.g., at the geothermal fields of the Salton Trough [Brodsky and Lajoie, 2013; Hauksson *et al.*, 2013] and the Coso Geothermal Field (CGF), both in California. The CGF as a produced geothermal reservoir in a magmatic system, has an abundance of natural and induced seismicity, with natural seismicity arising from both tectonic and magmatic sources [Manley and Bacon, 2000; Hauksson and Unruh, 2007]. A volume of partial melt is thought to be present at as shallow as 5.5 km depth based on temperature gradients and rhyolite thermobarometry [Manley and Bacon, 2000; Monastero *et al.*, 2005]. The wealth of knowledge gained about the system over the last four decades provides a special opportunity to study the evolution of seismicity from pre-production characteristics to large-scale power production over a long time span.

Exploration at the CGF, which began in the 1970s and culminated with the drilling of the exploration well CGEH-1 (Sept.-Dec. 1977), is documented in a special issue of the Journal of Geophysical Research [Bacon and Duffield, 1980]. Two base-line microseismic surveys were conducted by Combs and Rotstein [1975] in summer 1974 and by Walter and Weaver [1980b] between September 1975 and September 1977. Both studies document a high level of local seismicity including several earthquake clusters. The area is among

the most seismically active areas in southern California and featured seven magnitude 5 and larger events during the period 1982–2001 within a 30 km radius around the geothermal field (Southern California Seismic Network (SCSN) catalog) (Figure 1, top and middle panels), however the largest events within the produced CGF itself are all smaller than M5.

Four geothermal power plants went online between 1987 and 1990 providing 270 MW installed capacity [Monastero, 2002]. Production peaked in the early 1990s and has slowly declined since (Figure 1, bottom panel). The seismicity induced by the operations in the field is monitored by a dedicated local seismic network (see Section 2). Induced seismicity as result of geothermal power production at Coso has been previously recognized [Malin, 1994; Feng and Lees, 1998; Lees, 1998]. Kaven et al. [2013, 2014] and Kaven et al. [in prep.] performed re-locations and a joint 3-D tomography of the 1996–2012 seismicity recorded by the local network and show clear spatial correlation between open-hole intervals in wells and diffuse seismicity within fault-bounded volumes. Julian et al. [Julian et al., 2009, 2010] also recognized earthquake sequences resulting from fluid movement out of a single well, 34-9RD2, during drilling.

In this study we analyze pre-production seismicity and compare it with seismicity during the production period from 1987 to 2013. To identify earthquake swarms among the current high level of seismicity during production we use a method that groups events into clusters by calculation of a multi-dimensional distance derived from relative timing, energy, and spatial separation [Zaliapin and Ben-Zion, 2013a]. After implementing and testing the method on the pre-production survey, we apply it to the seismicity catalogs covering the period 1981–2013. The identified clusters are analyzed with respect to their topological structure to identify features that may discriminate natural from induced earthquake sequences. In this study we define an earthquake cluster as a sequence of spatially and temporally related seismicity. They are categorized as mainshock-aftershock sequences where the largest event occurs at the beginning of a sequence (possibly preceded by few minor foreshocks). Typically, the magnitude difference between the mainshock and the largest aftershock is on the order of 1 [Båth, 1965]. If the largest magnitude event occurs in the middle of a cluster and does not stand out by a significant magnitude difference the cluster is called a swarm [Mogi, 1963].

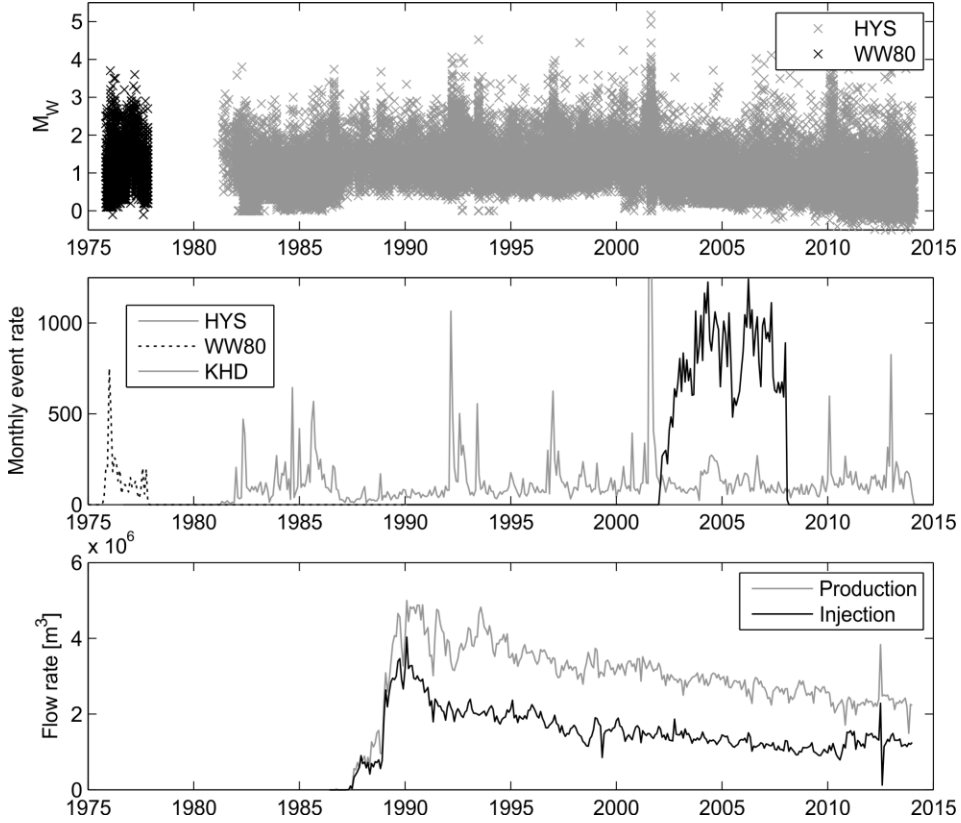


Figure 1: Production and seismic history at the CGF in study area A (Figure 2). (Top) Earthquakes from the HYS and Walter & Weaver (1980) catalogs, magnitude corrected according to Figure 3. Note the varying magnitude of completeness in the HYS catalog. (Middle) Seismic event rates from the WW80, HYS and KHD catalogs. (Bottom) Monthly production and injection rates of the CGF from 1981–2014 obtained from the California Department of Conservation.

2. SEISMOTECTONIC SETTING OF THE COSO GEOTHERMAL FIELD

Natural seismicity at the CGF is driven by extension and transtension along the Eastern California Shear Zone (ECSZ) that marks the transition from the strike-slip San Andreas Fault to the extensional Basin and Range Province. Accordingly, most focal mechanisms show normal or strike slip faulting [Hauksson and Unruh, 2007]. The high level of seismic activity in the Coso Range (Figure 1) can be partially attributed to the relative motion accommodated across the ECSZ, which is on the order of one fourth of the relative motion along the San Andreas Fault system [Unruh and Hauksson, 2009]. The Coso field is situated in the releasing step between the Little

Lake fault zone to the SW and the Wild Horse Mesa fault to the NE [Weaver and Hill, 1978; Walter and Weaver, 1980b]. Along that step $6.5 \pm 0.7 \text{ mm a}^{-1}$ of dextral shearing is observed [McClusky et al., 2001; Monastero et al., 2005]. Furthermore, it is suggested that some of the seismic activity can be linked to the presence of the volcanic system and the shallow brittle-ductile transition (BDT) [Hauksson and Unruh, 2007]. Previous workers have speculated that the episodic swarm activity can be attributed to upwelling of fluids emanating from below the BDT [Hauksson and Unruh, 2007]. Walter and Weaver [1980b] report several earthquake clusters occurring during their study period. The larger clusters beyond the geothermal field were identified as aftershock sequences at the edge of the study area. Close to one of those mainshock-aftershock sequences described by Walter and Weaver [1980b] two $M_L = 5.2$ and 5.8 events and accompanying aftershock sequences occurred in 1996 and 1998, respectively [Bhattacharyya et al., 1999]. Other clusters can be identified as swarm seismicity (Section 5.1), i.e., they are earthquake sequences that neither show a clear mainshock, nor the typical subsequent decline of aftershock activity [Mogi, 1963].

Feng and Lees [1998] analyzed earthquake focal mechanisms and identified a transition from a transtensional regime within the geothermal production area to a transpressional regime surrounding the reservoir. They postulated that the different stress regimes represent different geological blocks, evidenced also by different stress orientations. Fialko and Simons [2000] and Wicks et al. [2001] analyzed surface deformation using InSAR data. They found major subsidence in an area of 50 km^2 , with subsidence rates of $3\text{--}4 \text{ cm a}^{-1}$ and $10^6 \text{ m}^3 \text{a}^{-1}$ volume reduction [Fialko and Simons, 2000]. The modeled sources of the volume reduction are at 1–3 km depth, which agrees well with the depth of production and reinjection. They also noted an area of relative uplift in the south, possibly related to reinjection; Feng and Lees [1998] observed a clustering of potentially induced seismicity in this region. The sources modeled by Wicks et al. [2001] are slightly deeper at 3.1–4.7 km. While temperature reductions theoretically might play a role in the observed subsidence, they can be excluded to contribute substantially, since no large scale temperature reduction has been observed in the reservoir [Terra-Gen, pers. communication].

The lower boundary of seismicity is typically interpreted as evidence for the brittle-ductile transition (BDT) [Hauksson and Unruh, 2007]. Walter & Weaver [1980b] specifically remark that no indications of systematically shallower seismicity under the geothermal field could be found. Monastero et al. [2005] analyzed the maximum depth of seismicity from 40,000 events recorded across the geothermal field. They find a strong reduction of the depth of the deepest seismicity from around 10 km surrounding the field to as low as 3.5–4 km below the produced field. However, it remains doubtful if this observation is biased by the huge number of induced events, that typically occur in the immediate surroundings of the production and injection wells that reach down to about 3 km below surface. Since the depth of the BDT was determined from the 95% shallowest earthquakes, the large number of induced events might mask the actual BDT marked by fewer natural events occurring below the induced seismicity.

Although most studies agree that magma is the likely heat source of the geothermal system, there is debate about the depth of the magma. While the tomographic study by Hauksson and Unruh [2007] shows it to be deep seated below 10 km depth, compatible with geochronological analyses by Duffield et al. [1980], Monastero et al. [2005], Wilson et al. [2003], and Manley and Bacon [2000] argue it to be as shallow as 5 km based on inferences from shallower temperature logs or thermobarometry of the erupted rhyolite.

Studying earthquake swarms at Coso is especially interesting since they could be related to fluids entering the system under lithostatic pressure from below the otherwise self-sealing BDT [Vidale and Shearer, 2006; Hauksson and Unruh, 2007]. If the swarms at Coso are fluid-triggered, the physical processes of earthquake nucleation should be similar to fluid-induced seismicity. Following this assumption, the swarm seismicity at Coso should have characteristics similar to that of injection-induced seismicity (e.g., a spatio-temporal migration as the pore pressure perturbation propagates from the entry points below the BDT or perforated well sections, respectively).

3. DATA

In our analysis, we use three different catalogs that span the period from 1975 to 2013. These include the pre-production microseismic survey by Walter and Weaver [1980b] (WW80), the relocated catalog compiled from local network recordings from 2002 to 2007 [Kaven et al., 2014], hereafter referred to as KHD, and the catalog of the Southern California Seismic Network (SCSN) spanning the entire time interval from 1975–2013 [Hutton et al., 2010]. For the cluster analysis we use the relocations of the SCSN catalog by Hauksson et al. [2012], hereafter referred to as HYS, that are available for the period after 1981. We restrict our analysis to a rectangle bounded by $\{35.90^\circ < \text{latitude} < 36.15^\circ; -117.95^\circ < \text{longitude} < -117.65^\circ\}$ and term it study area A (Figure 2).

WW80: In September 1975 a network of 16 vertical-component seismometers was deployed around the geothermal field (Figure 2) [Walter and Weaver, 1980b]. Magnitudes were derived from a coda-length-magnitude relationship for central California. The events were located using the software HYPO71 [Lee and Lahr, 1975]. The whole catalog contains 4216 events [Walter and Weaver, 1980a] of which 2365 events are contained in study area A.

KHD: The KHD catalog [Kaven et al., 2013, 2014] and Kaven et al. [in prep.], is based on reprocessing of the recordings of the local seismic network operated at the CGF (Figure 2). The relocations were obtained using the code tomoDD, simultaneously solving for a 3-D velocity model. Moment magnitudes were computed by integrating the first displacement pulse. The catalog contains 57,000 events in study area A.

HYS: The HYS catalog [Hauksson et al., 2012] is based on the seismic recordings of the SCSN and reprocessed using the double-difference method. The original catalog is augmented by the latest dataset, covering the period of 07/2011–2013 [Hauksson et al., 2014]. The earthquake magnitudes are adopted from the SCSN catalog, described in detail by Hutton et al. [2010]. The catalog contains

52,000 events in study area A. For the study period 1981–2013 the SCSN catalog contains 202 events that are not contained in the HYS catalog and might have been rejected during the processing of the HYS catalog. Since these events are small, mostly below magnitude 1, this should have no influence on our analysis.

Figure 3 shows a cross-plot of earthquake magnitudes between the SCSN and WW80 catalogs and between the HYS and KHD catalogs. Subtracting 0.2 from the WW80 magnitudes yields an acceptable agreement between the catalogs. The magnitude of completeness given by Walter and Weaver [Walter and Weaver, 1980b] as $M_c = 1.5$ can therefore be assumed to be 1.3 when comparing with the magnitudes given in the SCSN catalog. We did not perform a formal magnitude of completeness study for the HYS and KHD catalogs, but have to note, that M_c varies over time for the HYS catalog (Figure 1a). For all analyses we use the full catalogs, not excluding events that are below a magnitude of completeness.

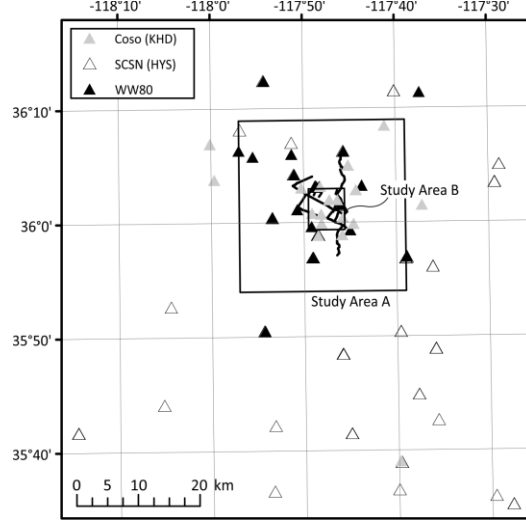


Figure 2: Seismic networks used to compile the WW80 catalog (black) and the KHD catalog (gray), and nearest stations of the SCSN used for the HYS catalog. Study areas A and B are outlined by boxes.

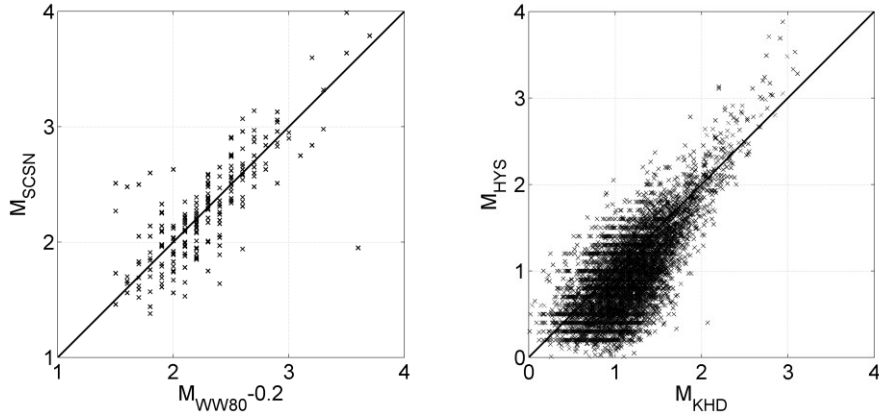


Figure 3: Crossplots of magnitudes between the SCSN and W80 catalogs after correcting WW80 by –0.2 (Left) and between the HYS and KHD catalogs (Right).

4. CLUSTER IDENTIFICATION

We analyze earthquake clustering in the seismic catalogs using the method described by Zaliapin and Ben-Zion [2013a]. It bases on nearest-neighbor distances computed in a time-space-energy domain. For each pair of events i and j , the multi-dimensional distance η_{ij} is computed using

$$\eta_{ij} = \begin{cases} t_{ij}(r_{ij})^d 10^{-bm_i}, & t_{ij} > 0 \\ \infty, & t_{ij} \leq 0 \end{cases}, \quad (1)$$

with inter-event time t_{ij} , inter-event distance r_{ij} , spatial dimension d , magnitude m and the b -value of the magnitude-frequency relation. In this study we use $d = 3$, since the studied seismicity occurs in a volume and depth variation of related seismicity is expected to be of the order of lateral variations; and $b = 1$, which is the average value for southern California [Hutton et al., 2010]. If η_{ij} is the

minimal multi-dimensional distance from event j to any other previous event, then event i is called the parent to offspring event j . Event j is then included in the cluster that contains event i . If η_{ij} is above the threshold the event is found to be unrelated to previous seismicity and it is assigned to a new cluster and the process repeats. Applying this procedure to a catalog, every event is part of a cluster with typically most clusters consisting of only one event. As discussed by Zaliapin and Ben-Zion [2013a], the nearest-neighbor-distance, which is the minimal value of η_{ij} for event j , shows a bimodal distribution, representing clustered and single earthquakes, respectively. The local minimum between the two peaks is used to set the threshold for η_{ij} to include an event to a cluster to $\log(\eta_{ij}) = -0.45$ (Figure 4). Since η_{ij} is computed by multiplying inter-event time and inter-event distance, it is small whenever one of the components is small, although the other might be relatively large. Therefore, events occurring during an active swarm may be included in a cluster although their geometrical inter-event distance is too large to be physically connected to the actual swarm. We therefore introduce a cutoff distance as five times the mean distance of all events in the considered cluster from the first event of the cluster. For events that occur beyond that threshold we set $\eta_{ij} = \infty$ to exclude it from the cluster. We do not introduce a cutoff in time for events occurring geometrically very close to previous events but after a long time of inactivity. Instead, these events are regarded as part of the declining activity analogous to aftershock sequences. Figure 5 shows the η_{ij} matrix and the identified clusters for the WW80 catalog.

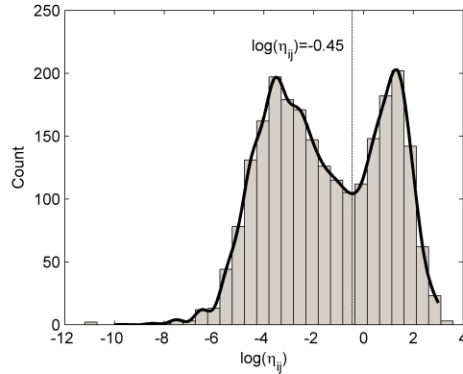


Figure 4: Histogram of the nearest-neighbor-distance $\min_j(\eta_{ij})$ for each event of the WW80 catalog. The minimum at $\log(\eta_{ij}) = -0.45$ is used as the cutoff value between single and clustered earthquakes.

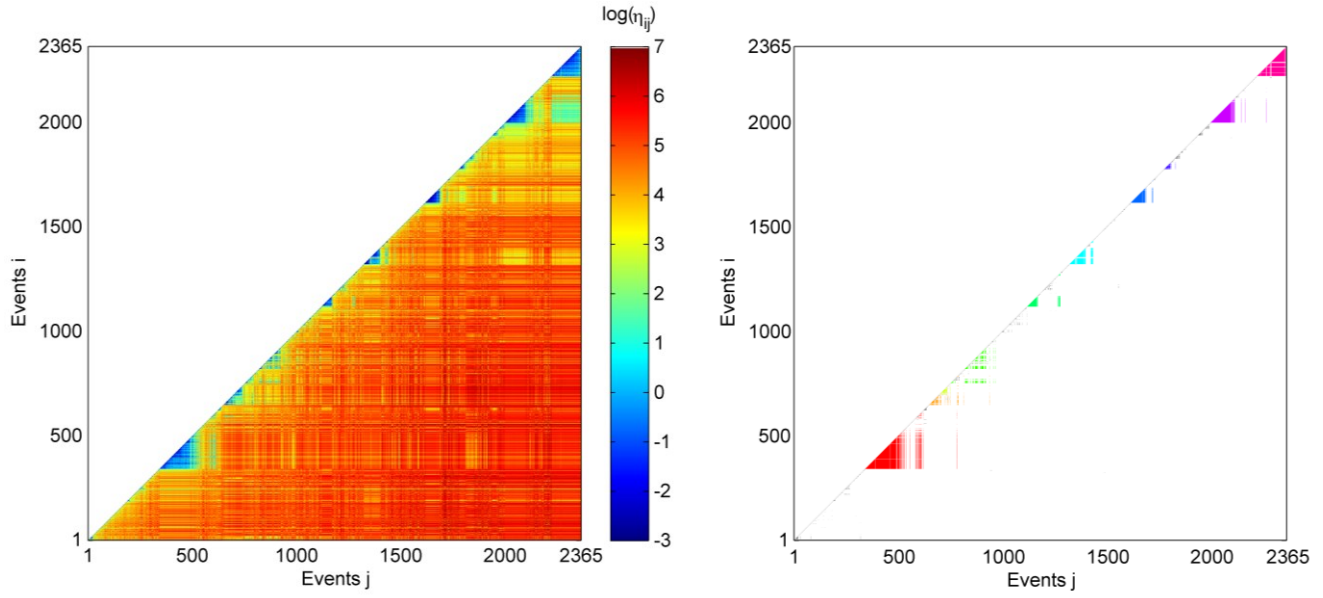


Figure 5: (Left) Inter-event space-time-energy distance matrix for the WW80 catalog. (Right) Matrix of identified clusters. Colored clusters each contain more than 20 events.

5. RESULTS

5.1. 1975–1977: PRE-PRODUCTION SEISMICITY

Out of the 2365 events of the WW80 catalog that occur within the study area A, 1613 (68 %) are part of a cluster and 752 events (32 %) are single events. For each cluster the hierarchy is implicitly obtained and it can be used to determine whether a cluster is an aftershock sequence or a seismic swarm. For that purpose Zaliapin and Ben-Zion [2013b] introduce a number of statistical parameter that describe

the cluster hierarchy. The leaf depth d for each event of a cluster is computed by counting the number of links between the first event of the cluster to the leafs, i.e. events that do not have offspring. Then, aftershock sequences are typically characterized by a small average leaf depth $\langle d \rangle$ on the order of 3. That means a mainshock has many direct offspring, but only few of them create offspring themselves. Swarms, in contrast, are built of chains of events, resulting in a high $\langle d \rangle$ on the order of 5 and larger. Naturally, $\langle d \rangle$ is dependent on the cluster size and tends to increase with more events forming a cluster. Therefore Zaliapin and Ben-Zion [2013b] introduce the normalized depth $\delta = \langle d \rangle \cdot N^{-0.5}$, where N is the number of events in a cluster.

Figure 6 shows magnitude-time and hierarchy plots for two similarly sized clusters; typical examples of a mainshock-aftershock sequence and a swarm. The mainshock-aftershock sequence has two mainshocks and overall 16 events. Its average leaf depth $\langle d \rangle = 1.7$ and $\delta = 0.43$. In contrast, the swarm with 14 events has $\langle d \rangle = 4.0$ and $\delta = 1.1$.

Another topological parameter is the Family branching number B , obtained by dividing the number of links between parent and offspring events by the number of events that have links to offspring. The swarm in Figure 6 has 8 events that have in total 13 offspring, yielding $B = 1.625$. In contrast, the mainshock-aftershock sequence has $B = 3.0$ due to the large number of events which are direct offspring of the mainshocks. Since these aftershocks have a small magnitude, their area of influence is small compared to the mainshocks, and only few further offspring are attributed to them.

In total, 21 clusters were identified in the WW80 catalog that have more than 10 events (Figure 7a). Three of the clusters were identified as mainshock-aftershock sequences, 16 clusters were identified as swarms and two clusters could not be classified as either with certainty.

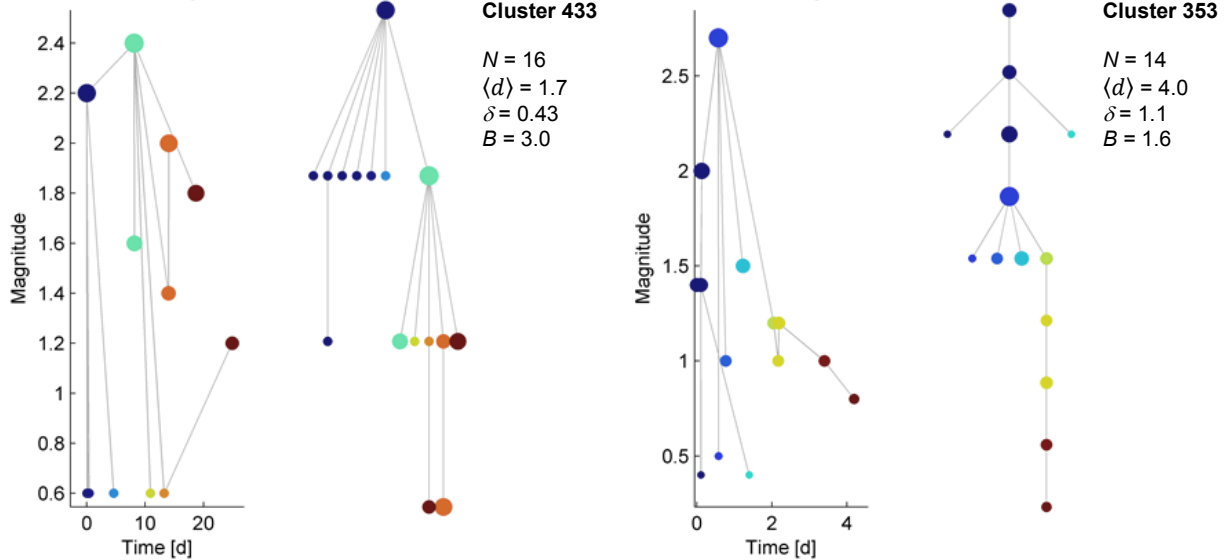


Figure 6: Magnitude-time and hierarchy plots for two smaller clusters with lines connecting each cluster event with its nearest neighbor. Dot size represents event magnitude, dot color the timing within the cluster as defined by the magnitude-time plots. Cluster 433 (Left) is two connected mainshock-aftershock sequences with many direct offspring of the two mainshocks, whereas cluster 353 (Right) is a typical swarm with long chains of events.

5.2. 1981–2013: DOUBLE-DIFFERENCE CATALOG, HYS

Like the WW80 catalog, the HYS catalog covers the pre-production period prior to 1987, containing 9,361 events recorded before 1987. Although these two catalogs overlap, in the HYS catalog only the period from ~1982 to 1987 is covered with a magnitude of completeness similar to the WW80 catalog. The vast majority of 42,967 events in the HYS catalog were recorded during the co-produced period since 1987. Due to the large number of events in the catalog, we restrict our analysis to clusters that contain at least 20 events. For the cluster analysis we split the catalog into the pre-production period (1981–1986) and the co-production period (1987–2013). The algorithm identified 42 clusters in the pre-production and 218 cluster in the co-production phases (Figure 7b and d). Among them were 2 and 40 clusters, respectively, that resembled mainshock-aftershock sequences. They are characterized by the largest magnitude event occurring at the beginning of the sequence and a large magnitude difference from the largest to the second largest event. All other clusters were identified as swarm-like with the largest event in the middle of the sequence and no events standing out as a particular mainshock [Mogi, 1963].

5.3. 2002–2007: LOCAL NETWORK CATALOG, KHD

The KHD catalog covers a much shorter time span from 2002 to 2007. As it has a lower magnitude of completeness, it contains about the same number of events as the HYS catalog. The cluster identification algorithm identified 280 clusters with more than 20 events and among them are 26 mainshock-aftershock sequences (Figure 7c).

6. DISCUSSION

In the following discussion, we will subdivide study area A into study area B below the produced geothermal field and defined by $\{35.99^\circ < \text{latitude} < 36.05^\circ; -117.825^\circ < \text{longitude} < -117.760^\circ\}$ (Figure 7) and study area A-B, the area in A but not in B around the produced field. We reduce the coordinates of the clusters to that of the median coordinates of all events contained in the cluster and ignore its spatial extent. To compare the seismicity clusters located in study areas A-B and B, we derive the topological parameters normalized leaf depth δ and the family branching number B for each cluster (see Section 5.1). Clear mainshock-aftershock sequences were removed for the analysis based on position of the largest event of the cluster at the beginning, allowing for few foreshocks, and the magnitude difference Δ_A between the largest to the second largest event. We compute boxplots for the four catalogs as presented in Figure 7 and separated for study areas A-B and B for the parameters depth below sea level z , normalized leaf depth δ and family branching number B , respectively (Figure 8). As the WW80 catalog has only few samples computing boxplots would be meaningless. Nevertheless, the results for the individual clusters are added to the plots for comparison with the other catalogs.

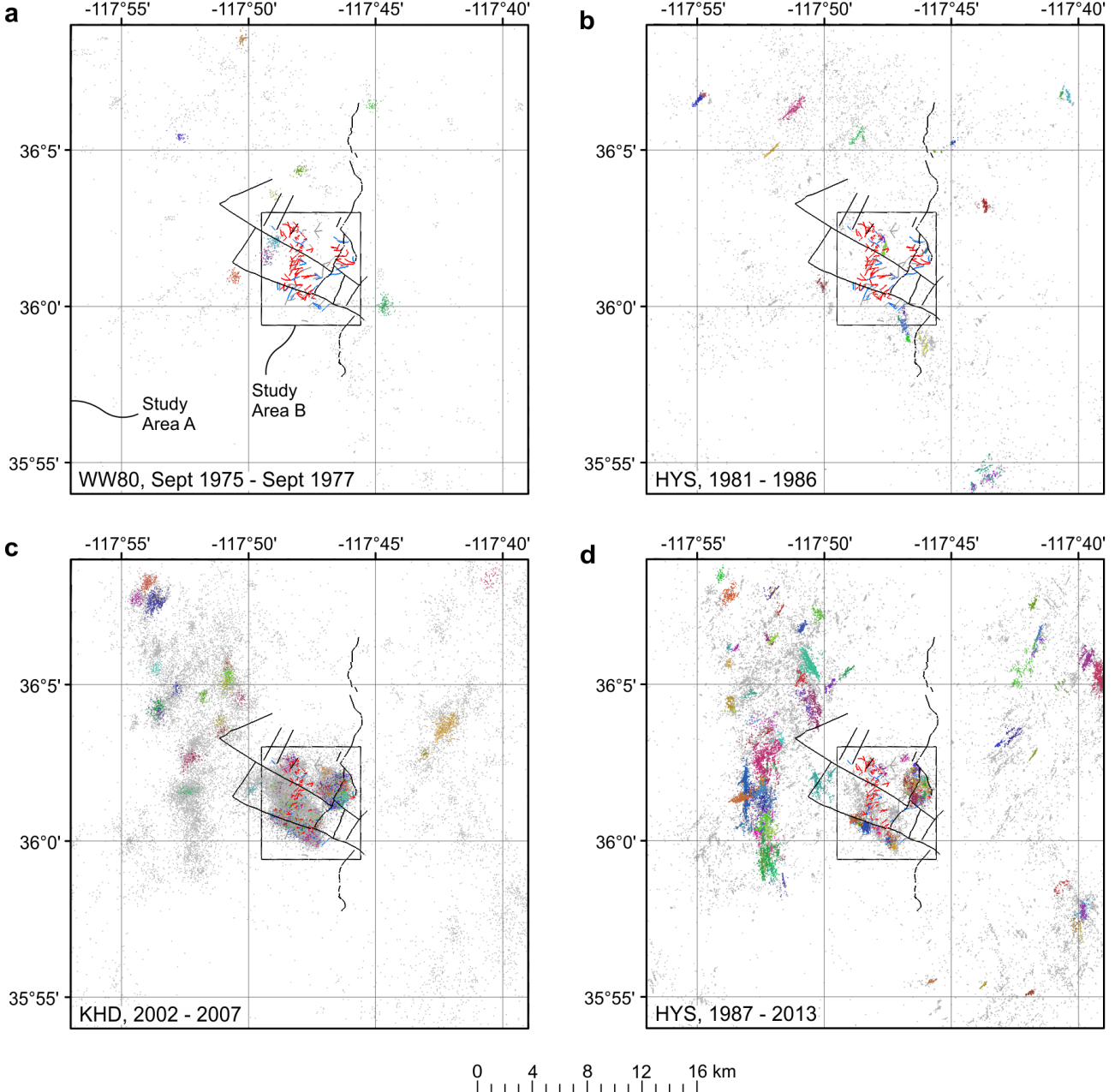


Figure 7: Map views of the analyzed catalogs with large clusters ($N > 20$ events for WW80 catalog, and $N > 50$ events for HYS and KHD catalogs) identified by distinct colors. The outline of each figure coincides with study area A. The current production (red) and injection wells (blue) and surface traces of major faults (black) are superimposed for reference. Clusters are drawn superimposed on the remaining seismicity for clarity.

To quantify the statistical significance of the observed differences, we perform Kolmogorov-Smirnov (K-S) tests [Jensen *et al.*, 2000] on the determined cluster parameters of two sets of two samples: study areas A-B and B for both catalogs and the time periods 1981-1986 and 1987-2013 for the HYS catalog. The tests yield a probability for the validity of the null hypothesis, i.e., that the measured parameters for both subsets stem from the same distribution and the measured differences are random sampling errors (Tables 1 and 2).

Figure 8a shows the boxplots for depth z . While in study area A-B z varies around 4 km below sea level (bsl) for all catalogs, the situation is more complicated in study area B. In the pre-production period WW80 has two clusters at 6 km and HYS has seven clusters at a median of 2.6 km bsl. The K-S test does not reject the null hypothesis, i.e. the differences in cluster depths between both study areas are not statistically significant. In the co-production period, the HYS catalog has a median of 1.8 km with a narrow standard deviation and the KHD catalog places the clusters at 0.6 km bsl, which are strong differences to study area A-B, as confirmed by the K-S test. The difference in resolved depths between the HYS and KHD catalogs in study area B can be related to the used seismic networks, with the local network used for the KHD catalog focused on study area B rather than study area A-B. The average surface elevation at Coso is on the order of 1.5 km, placing the average cluster according to the KHD catalog at about 2 km depth below surface. For reference, the maximum well depths are added to Figure 8a. They show a good agreement with the co-production cluster depths given by both catalogs. It appears that study area B has slightly shallower seismicity pre-production and significantly shallower seismicity co-production and correlates well with borehole depths. Based on the pre-production seismicity it cannot be concluded that the clusters are systematically shallower in study area B than in study area A-B.

The normalized leaf depth δ (Figure 8b) shows an uneven image. The HYS catalog shows a slight reduction of δ in both study areas going from the pre- to the co-production period. According to the K-S test, δ cannot be distinguished in both study areas but changes with time. For the KHD catalog a difference of δ between the study areas is observed, which is significant according to the K-S test. The family branching number B (Figure 8c) shows no difference between both study areas pre-production, but significant differences in both co-production catalogs, which show a smaller B in the produced study area B than around the produced field. This means that clusters in study area B are slightly more dissimilar in branching behavior from mainshock-aftershock sequences than are clusters in study area A-B, i.e. the swarthy behavior with no big events particularly standing out and parent-offspring relation dominated by linear chains is enhanced. No significant change of B is found between the pre- and co-production periods.

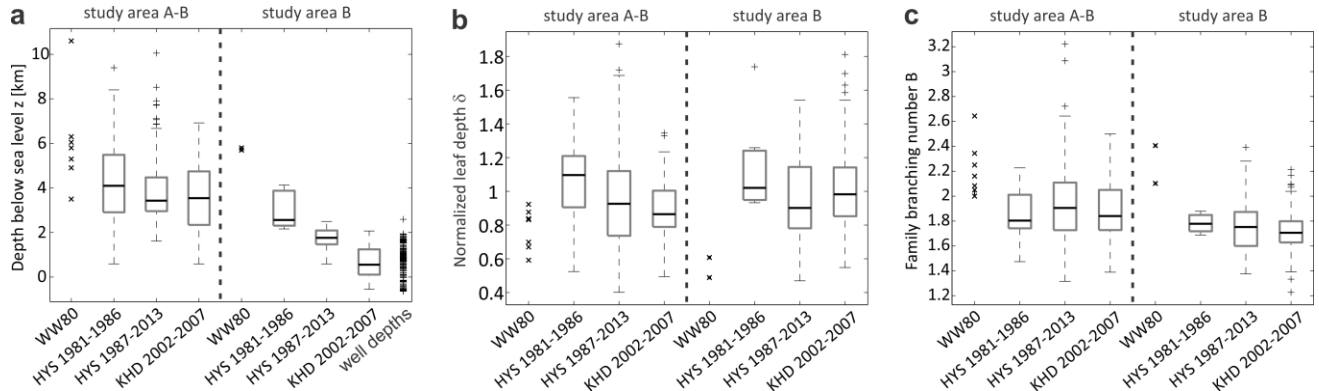


Figure 8: Boxplots of depth, normalized leaf depth δ and family branching number B of the clusters identified from the catalogs for study areas A-B and B. Aftershock sequences were removed for this analysis. Due to small number of clusters in the WW80 catalogs, only the individual quantities are plotted. In subfigure (a) the depths of the wells in study area B are plotted for comparison.

Statistic S	Catalog	Samples (A-B)	Median (A-B)	Samples (B)	Median (B)	P	Decision at 5 % level
Depth below sea level z	HYS 1981-1986	33	4.1	7	2.6	0.09	Do not reject
	HYS 1987-2013	141	3.4	32	1.8	4.9E-22	Reject
	KHD 2002-2007	62	3.5	192	0.6	1.3E-27	Reject
Normalized leaf depth δ	HYS 1981-1986	33	1.1	7	1.0	0.58	Do not reject
	HYS 1987-2013	141	0.9	32	0.9	0.87	Do not reject
	KHD 2002-2007	62	0.9	192	1.0	1.1E-3	Reject
Family branching number B	HYS 1981-1986	33	1.8	7	1.8	0.13	Do not reject
	HYS 1987-2013	141	1.9	32	1.8	1.2E-3	Reject
	KHD 2002-2007	62	1.8	192	1.7	4.4E-5	Reject
Magnitude difference Δ_A	HYS 1981-1986	33	0.19	7	0.24	0.44	Do not reject
	HYS 1987-2013	141	0.16	32	0.19	0.39	Do not reject
	KHD 2002-2007	62	0.14	192	0.15	0.76	Do not reject

Table 1: Results of Kolmogorov-Smirnov tests of the null hypothesis: The statistic S is the same for study areas A-B and B.

Statistic S	Area	Samples 1981-1986	Median 1981-1986	Samples 1987-2013	Median 1987-2013	P	Decision at 5 % level
Depth below sea level z	A-B	33	4.1	141	3.4	0.07	Do not reject
	B	7	2.6	32	1.8	6.6E-4	Reject
Normalized leaf depth δ	A-B	33	1.1	141	0.9	0.02	Reject
	B	7	1.0	32	0.9	0.05	Reject
Family branching number B	A-B	33	1.8	141	1.9	0.39	Do not reject
	B	7	1.8	32	1.8	0.42	Do not reject
Magnitude difference Δ_A	A-B	33	0.19	141	0.16	0.11	Do not reject
	B	7	0.24	32	0.19	0.79	Do not reject

Table 2: Results of Kolmogorov-Smirnov tests of the null hypothesis: The statistic S is the same for the time periods 1981-1987 and 1986-2013 as determined from the HYS catalog.

Zaliapin and Ben-Zion [2013b] also propose the magnitude difference Δ_A between the largest and second largest event as a characteristic parameter of a cluster. This is useful mainly to discriminate mainshock-aftershock sequences, with a large Δ_A (Båth's law) from swarms with small Δ_A . No significant difference in Δ_A was found between clusters in both study areas and time periods with median Δ_A being on the order of 0.2 for all clusters.

While the WW80 catalog and also the pre-production part of the HYS catalog, show some level of seismicity and even few clusters in study area B, study area B strongly stands out as the most active volume during the co-production period and that activity appears to be spatially associated with the open-hole interval of wells. It is therefore plausible to conclude that the vast majority of seismicity recorded in this region is induced. The sharp delineation of the highly active area to all sides can be used to further conclude that the zone perturbed by the operation of the geothermal plant is limited to approximately the outline of study area B.

Possible causes for the differences in B and δ between study areas A-B and B, other than their nature as natural versus induced seismicity, are the extreme thermal gradient and elevated heat flow around the produced geothermal field [Combs, 1980]. Indeed, Zaliapin and Ben-Zion [2013b] find a systematically smaller value of B for hot regions than for cold regions in southern California. In their interpretation this is linked to the more pronounced role of ductile processes in hot systems. However, it has also been shown before that ductile processes, evidenced by aseismic deformation, play an important role at sites of deep fluid injection in fractured reservoirs [Schmittbuhl et al., 2014; Schoenball et al., 2014].

7. CONCLUSIONS

The large amount of natural and induced seismicity and the wealth of knowledge about the CGF collected over the past several decades make it an ideal site to study natural and induced seismicity in a comparative manner. We compared clusters inside and around the produced geothermal field during pre- and co-production periods by a cluster identification algorithm based on the inter-event distance in the space-time-energy domain. Through analysis of the topological parameters family branching number B and normalized leaf depth δ of the identified clusters, we find significant differences in B and inconclusive differences in δ both study areas.

ACKNOWLEDGEMENTS

We thank the Navy GPO and Terra-Gen for permission to use their seismic and field data and the Southern California Seismic Network for their earthquake catalog. This work is supported by Temple University and the USGS Energy Program's Geothermal Project. M. Schoenball is financed by Cooperative Agreement Number G13AC00283 from the USGS to Temple University: Geothermal Systems in the Western U.S. We thank Andrea Llenos and David Shelly for helpful comments on the manuscript.

REFERENCES

- Bacon, C. R., and W. A. Duffield (1980), Coso Geothermal Area, *J. Geophys. Res. Solid Earth*, 85(B5), 2379, doi:10.1029/JB085iB05p02379.
- Båth, M. (1965), Lateral inhomogeneities of the upper mantle, *Tectonophysics*, 2(6), 483–514, doi:10.1016/0040-1951(65)90003-X.
- Bhattacharyya, J., S. Gross, J. Lees, and M. Hastings (1999), Recent Earthquake Sequences at Coso: Evidence for Conjugate Faulting and Stress Loading near a Geothermal Field, *Bull. Seismol. Soc. Am.*, 89(3), 785–795.
- Brodsky, E. E., and L. J. Lajoie (2013), Anthropogenic Seismicity Rates and Operational Parameters at the Salton Sea Geothermal Field., *Science*, 341, 543, doi:10.1126/science.1239213.

- Combs, J. (1980), Heat flow in the Coso Geothermal Area, Inyo County, California, *J. Geophys. Res.*, 85(B5), 2411, doi:10.1029/JB085iB05p02411.
- Combs, J., and Y. Rotstein (1975), Microearthquake Studies at the Coso Geothermal Area, China Lake, California, in *Second U.N. Symposium on the Development and Use of Geothermal Resources*, pp. 909–916, San Francisco, California, USA.
- Duffield, W. A., C. R. Bacon, and G. B. Dalrymple (1980), Late Cenozoic volcanism, geochronology, and structure of the Coso Range, Inyo County, California, *J. Geophys. Res.*, 85(B5), 2381, doi:10.1029/JB085iB05p02381.
- Ellsworth, W. L. (2013), Injection-induced earthquakes., *Science*, 341, 1225942, doi:10.1126/science.1225942.
- Feng, Q., and J. M. Lees (1998), Microseismicity, stress, and fracture in the Coso geothermal field, California, *Tectonophysics*, 289(1-3), 221–238, doi:10.1016/S0040-1951(97)00317-X.
- Fialko, Y., and M. Simons (2000), Deformation and seismicity in the Coso geothermal area, Inyo County, California: Observations and modeling using satellite radar interferometry, *J. Geophys. Res.*, 105(B9), 21781, doi:10.1029/2000JB900169.
- Hauksson, E., and J. Unruh (2007), Regional tectonics of the Coso geothermal area along the intracontinental plate boundary in central eastern California: Three-dimensional Vp and Vp/Vs models, spatial-temporal seismicity patterns, and seismogenic deformation, *J. Geophys. Res.*, 112(B6), B06309, doi:10.1029/2006JB004721.
- Hauksson, E., W. Yang, and P. M. Shearer (2012), Waveform Relocated Earthquake Catalog for Southern California (1981 to June 2011), *Bull. Seismol. Soc. Am.*, 102(5), 2239–2244, doi:10.1785/0120120010.
- Hauksson, E. et al. (2013), Report on the August 2012 Brawley Earthquake Swarm in Imperial Valley, Southern California, *Seismol. Res. Lett.*, 84(2), 177–189, doi:10.1785/0220120169.
- Hauksson, E., W. Yang, and P. M. Shearer (2014), Waveform Relocated Earthquake Catalog for Southern California, Available from: <http://www.data.scec.org/research-tools/alt-2011-dd-hauksson-yang-shearer.html>
- Hutton, K., J. Woessner, and E. Hauksson (2010), Earthquake Monitoring in Southern California for Seventy-Seven Years (1932–2008), *Bull. Seismol. Soc. Am.*, 100(2), 423–446, doi:10.1785/0120090130.
- IEA (2011), *Technology Roadmap: Geothermal Heat and Power*, IEA Technology Roadmaps, OECD Publishing.
- Jensen, J. L., L. W. Lake, P. W. M. Corbett, and D. J. Goggin (2000), *Statistics for Petroleum Engineers and Geoscientists*, 2nd ed., Elsevier, Amsterdam.
- Julian, B. R., G. R. Foulger, and F. C. Monastero (2009), Seismic monitoring of EGS stimulation tests at the Coso Geothermal Field, California, using microearthquake locations and moment tensors, in *Stanford Geothermal Workshop*, p. 10.
- Julian, B. R., G. R. Foulger, F. C. Monastero, and S. Bjornstad (2010), Imaging hydraulic fractures in a geothermal reservoir, *Geophys. Res. Lett.*, 37(7), L07305, doi:10.1029/2009GL040933.
- Kaven, J. O., S. H. Hickman, and N. C. Davatzes (2013), Micro-seismicity within the Coso Geothermal Field, California, from 1996–2012, in *Stanford Geothermal Workshop*, p. 10.
- Kaven, J. O., S. H. Hickman, and N. C. Davatzes (2014), Micro-seismicity and seismic moment release within the Coso Geothermal Field, California, in *Stanford Geothermal Workshop*, p. 10.
- Lee, W. H. K., and J. C. Lahr (1975), *HYPO71 (revised): A computer program for determining hypocenter, magnitude and first motion pattern of local earthquakes*, Open-File Report 75-311, Menlo Park, California.
- Lees, J. M. (1998), Multiplet analysis at Coso Geothermal, *Bull. Seismol. Soc. Am.*, 88(5), 1127–1143.
- Majer, E. L., R. Baria, M. Stark, S. Oates, J. J. Bommer, B. Smith, and H. Asanuma (2007), Induced seismicity associated with enhanced geothermal systems, *Geothermics*, 36(3), 185–222, doi:DOI 10.1016/j.geothermics.2007.03.003.

- Malin, P. E. (1994), The seismology of extensional hydrothermal systems, *GRC Trans.*, 18, 17–22.
- Manley, C. R., and C. R. Bacon (2000), Rhyolite Thermobarometry and the Shallowing of the Magma Reservoir, Coso Volcanic Field, California, *J. Petrol.*, 41(1), 149–174, doi:10.1093/petrology/41.1.149.
- McClusky, S. C., S. C. Bjornstad, B. H. Hager, R. W. King, B. J. Meade, M. M. Miller, F. C. Monastero, and B. J. Souter (2001), Present day kinematics of the Eastern California Shear Zone from a geodetically constrained block model, *Geophys. Res. Lett.*, 28(17), 3369–3372, doi:10.1029/2001GL013091.
- Mogi, K. (1963), Some Discussions on Aftershocks, Foreshocks and Earthquake Swarms - the Fracture of a Semi-infite Body Caused by an Inner Stress Origin and Its Relation to the Earthquake Phenomena (3), *Bull. Earthq. Res. Inst.*, 41, 615–658.
- Monastero, F. C. (2002), Model for Success, *GRC Bull.*, 188–194.
- Monastero, F. C., A. M. Katzenstein, J. S. Miller, J. R. Unruh, M. C. Adams, and K. Richards-Dinger (2005), The Coso geothermal field: A nascent metamorphic core complex, *Geol. Soc. Am. Bull.*, 117(11), 1534, doi:10.1130/B25600.1.
- Schmittbuhl, J., O. Lengliné, F. Cornet, N. Cuenot, and A. Genter (2014), Induced seismicity in EGS reservoir: the creep route, *Geotherm. Energy*, 2(1), 14, doi:10.1186/s40517-014-0014-0.
- Schoenball, M., L. Dorbath, E. Gaucher, J. F. Wellmann, and T. Kohl (2014), Change of stress regime during geothermal reservoir stimulation, *Geophys. Res. Lett.*, 41(4), 1163–1170, doi:10.1002/2013GL058514.
- Unruh, J., and E. Hauksson (2009), Seismotectonics of an evolving intracontinental plate boundary, southeastern California, *Geol. Soc. Am. Spec. Pap.*, 447, 351–372, doi:10.1130/2009.2447(16).
- Vidale, J. E., and P. M. Shearer (2006), A survey of 71 earthquake bursts across southern California: Exploring the role of pore fluid pressure fluctuations and aseismic slip as drivers, *J. Geophys. Res.*, 111(B5), B05312, doi:10.1029/2005JB004034.
- Walter, A. W., and C. S. Weaver (1980a), *Catalog of earthquakes in the Coso Range and vicinity, southern California*, Open-File Report 80-85, U.S. Geological Survey, Menlo Park, California.
- Walter, A. W., and C. S. Weaver (1980b), Seismicity of the Coso Range, California, *J. Geophys. Res.*, 85(B5), 2441, doi:10.1029/JB085iB05p02441.
- Weaver, C. S., and D. P. Hill (1978), Earthquake swarms and local crustal spreading along major strike-slip faults in California, *Pure Appl. Geophys.*, 117(1-2), 51–64, doi:10.1007/BF00879733.
- Wicks, C. W., W. Thatcher, F. C. Monastero, and M. A. Hasting (2001), Steady state deformation of the Coso Range, east central California, inferred from satellite radar interferometry, *J. Geophys. Res.*, 106(B7), 13769, doi:10.1029/2001JB000298.
- Wilson, C. K., C. H. Jones, and H. J. Gilbert (2003), Single-chamber silicic magma system inferred from shear wave discontinuities of the crust and uppermost mantle, Coso geothermal area, California, *J. Geophys. Res.*, 108(B5), 2226, doi:10.1029/2002JB001798.
- Zaliapin, I., and Y. Ben-Zion (2013a), Earthquake clusters in southern California I: Identification and stability, *J. Geophys. Res. Solid Earth*, 118(6), 2847–2864, doi:10.1002/jgrb.50179.
- Zaliapin, I., and Y. Ben-Zion (2013b), Earthquake clusters in southern California II: Classification and relation to physical properties of the crust, *J. Geophys. Res. Solid Earth*, 118(6), 2865–2877, doi:10.1002/jgrb.50178.
- Zang, A., V. Oye, P. Jousset, N. Deichmann, R. Gritto, A. McGarr, E. Majer, and D. Bruhn (2014), Analysis of induced seismicity in geothermal reservoirs – An overview, *Geothermics*, 52, 6–21, doi:10.1016/j.geothermics.2014.06.005.